

RESEARCH ARTICLE

Open Access



# Applying arterial enhancement fraction (AEF) texture features to predict the tumor response in hepatocellular carcinoma (HCC) treated with Transarterial chemoembolization (TACE)

Xiaonan Mao<sup>1</sup>, Yan Guo<sup>2</sup>, Feng Wen<sup>1</sup>, Hongyuan Liang<sup>1</sup>, Wei Sun<sup>1</sup> and Zaiming Lu<sup>1\*</sup>

## Abstract

**Background:** To evaluate the application of Arterial Enhancement Fraction (AEF) texture features in predicting the tumor response in Hepatocellular Carcinoma (HCC) treated with Transarterial Chemoembolization (TACE) by means of texture analysis.

**Methods:** HCC patients treated with TACE in Shengjing Hospital of China Medical University from June 2018 to December 2019 were retrospectively enrolled in this study. Pre-TACE Contrast Enhanced Computed Tomography (CECT) and imaging follow-up within 6 months were both acquired. The tumor responses were categorized according to the modified RECIST (mRECIST) criteria. Based on the CECT images, Region of Interest (ROI) of HCC lesion was drawn, the AEF calculation and texture analysis upon AEF values in the ROI were performed using CT-Kinetics (C.K., GE Healthcare, China). A total of 32 AEF texture features were extracted and compared between different tumor response groups. Multi-variate logistic regression was performed using certain AEF features to build the differential models to predict the tumor response. The Receiver Operator Characteristic (ROC) analysis was implemented to assess the discriminative performance of these models.

**Results:** Forty-five patients were finally enrolled in the study. Eight AEF texture features showed significant distinction between Improved and Un-improved patients ( $p < 0.05$ ). In multi-variate logistic regression, 9 AEF texture features were applied into modeling to predict "Improved" outcome, and 4 AEF texture features were applied into modeling to predict "Un-worsened" outcome. The Area Under Curve (AUC), diagnostic accuracy, sensitivity, and specificity of the two models were 0.941, 0.911, 1.000, 0.826, and 0.824, 0.711, 0.581, 1.000, respectively.

**Conclusions:** Certain AEF heterogeneous features of HCC could possibly be utilized to predict the tumor response to TACE treatment.

**Keywords:** AEF, Texture analysis, Heterogeneity, Tumor response, TACE, HCC

\* Correspondence: [luzm@sj-hospital.org](mailto:luzm@sj-hospital.org)

<sup>1</sup>Department of Radiology, Shengjing hospital of China Medical University, 12# floor at 1# building, 39 Huaxiang Road, Shenyang City 110000, Liaoning Province, China

Full list of author information is available at the end of the article



© The Author(s). 2021 **Open Access** This article is licensed under a Creative Commons Attribution 4.0 International License, which permits use, sharing, adaptation, distribution and reproduction in any medium or format, as long as you give appropriate credit to the original author(s) and the source, provide a link to the Creative Commons licence, and indicate if changes were made. The images or other third party material in this article are included in the article's Creative Commons licence, unless indicated otherwise in a credit line to the material. If material is not included in the article's Creative Commons licence and your intended use is not permitted by statutory regulation or exceeds the permitted use, you will need to obtain permission directly from the copyright holder. To view a copy of this licence, visit <http://creativecommons.org/licenses/by/4.0/>. The Creative Commons Public Domain Dedication waiver (<http://creativecommons.org/publicdomain/zero/1.0/>) applies to the data made available in this article, unless otherwise stated in a credit line to the data.

## Background

Through the means of chemoinfusion and embolization, transarterial chemoembolization (TACE) has become one of the standard therapeutic options in the treatment of hepatocellular carcinoma (HCC) [1–3]. However, despite the rapid development of medicines and interventional devices, unbenefited patients to TACE still exist. These patients have always presented a great challenge to interventional radiologists in terms of both time and cost. A scientific prediction of tumor response before TACE would be very helpful in the integrated management of HCC.

According to the current guidelines on HCC management, mRECIST criteria [4] is used to judge tumor response based on specific imaging findings. The typical imaging finding of HCC lies in the enhancement pattern of arterial wash-in and portal/venous wash-out [1, 2, 4]. When HCC develops, the portal supply decreases, while the arterial supply increases and becomes more and more predominant [5–7]. The unique changes in perfusion status of the disease enable the application of perfusion analysis in HCC. Currently, with the development of computer engineering, arterial enhancement fraction (AEF), which reflects the ratio of the arterial supply to the portal supply, can be derived from routine enhanced CT images by aligning and subtracting unenhanced images from arterial and portal images [8, 9]. This provides us with a new method of perfusion analysis without subjecting patients to extra scanning and radiation exposure.

Different from traditional imaging analyses, which usually view the tumor as a whole, texture analysis disassembles the whole tumor into a number of independent pixels. Each pixel's color scales (Perfusion values) can then be converted into high-dimensional quantitative data [10–12]. By a series of statistical calculation, multiple microscopic texture features can be extracted and further investigated in combination with clinical or histological findings [13, 14]. With an interest in exploring this new technology, the present study used the method of texture analysis to evaluate the application of AEF in predicting tumor response in HCC treated with TACE.

## Methods

### Patient management

This retrospective study obtained the approval from the institutional ethics committee of our hospital before implementation. Patients were recruited among the HCC patients treated in Shengjing hospital from June 2018 to December 2019. The step-by-step inclusion process involved the following criteria: (1) A diagnosis of liver cancer; (2) Aged 30~90; (3) Nonpregnant (for female patients); (4) CECT was acquired; (5) HCC was defined;

(6) TACE was performed; (7) Imaging follow-up was conducted. The exclusion criteria included: (1) Uncorrectable artifacts; (2) Unmatched planes between phases; (3) Multiple HCCs (> 5); (4) Tiny HCC (< 1 cm); (5) Portal vein tumor thrombosis (PVTT) or portal vein cavernous transformation (PVCT); (6) Visible arterial-vein shunt (AVS); (7) Request to quit the study by the patient. Age, gender, hepatitis type, alcoholic background and family history of HCC were recorded. Liver function, renal function, coagulation function, ammonia, and alpha-fetoprotein (AFP) were tested. The China Staging System [1], Barcelona Staging System [2], and Child-Pugh Scoring system [15, 16] were used for integrated assessment.

Contrast enhanced imaging was acquired through a follow-up appointment that occurred within 6 months after TACE. The follow-up images together with the pre-TACE images were reviewed by two interventional radiologists who were neither co-authors, study designers, nor participants and were kept blind to the purpose of this study. The two radiologists were professionals in the interventional oncology field and had at least 5 years of working experience in abdominal imaging. They were tasked with classifying the tumor response in compliance with the modified RECIST (mRECIST) criteria [4] and with categorizing the outcomes of patients as Complete Remission (CR: The disappearance of any intratumoral arterial enhancement in all target lesions), Partial Response (PR: A decrease of at least 30% in the sum of the diameters of viable target lesions), Progressive Disease (PD: An increase of at least 20% in the sum of the diameters of viable target lesions) and Stable Disease (SD: A status that fits in between PR and SD but not qualify for either one) respectively.

### Image processing

CT scans were performed on a 128 row multi-detector CT (iCT 256, Philips, the Netherlands) with the scanning parameters as follows: Tube voltage 100kVp; Automatic tube current modulation; Pitch 0.993; Rotation time 0.5 s; Collimation 128 × 0.635; FOV 350 × 350 mm; Pixel size 0.8 × 0.8 mm; Plane thickness 3 mm. The enhanced images were acquired at the specific time points after the bolus injection of contrast (Visipaque 270, GE, Ireland): Arterial phase 23 s; Portal phase 45 s; Delay phase 120 s. The volume of contrast was calculated by 1.2 ml/kg on body weight. The injection rate was 4.5 ml/s, followed by a 20 ml saline flush.

CECT images of DICOM format were downloaded from the CT workstation and loaded into CT-Kinetics program (C.K., GE Healthcare, China). In order to overcome difficulties in controlling breath-holding in imaging patients, 3D non-rigid motion registration was applied to improve the possibility of a good match

between images of different phases. The aorta was chosen as the input artery, while the portal vein was chosen as the input vein. The density-time curve was obtained using a dual maximum slope model [17, 18]. The colored AEF map was generated automatically based on a pixel-by-pixel calculation of  $CT_a - CT_u / CT_p - CT_u$  ( $CT_u$ : unenhanced CT value,  $CT_a$ : arterial CT value;  $CT_p$ : portal CT value).

The Region of Interest (ROI) of HCC was manually delineated along the tumor outline on the largest axial plane. The two interventional radiologists conducted the ROI delineation, with a compromise agreement if any inconsistency existed. A total of 32 AEF texture features were extracted through automatic statistical calculations, including Intensity-Based Statistical (IBS) features (MinIntensity, MaxIntensity, MedianIntensity, MeanValue, StdDeviation, Variance, VolumeCount, VoxelValueSum, Range, MeanDeviation, RelativeDeviation), Intensity-Based Histogram (IBH) features (Skewness, Kurtosis, Uniformity, Energy, Entropy), Gray-Level Co-occurrence Matrix (GLCM) features (Inertia, Correlation, InverseDifferenceMoment, ClusterShade, ClusterProminence, HaralickCorrelation), and Gray-Level Run-Length Matrix (GLRLM) features (ShortRunEmphasis, LongRunEmphasis, GreyLevelNonuniformity, RunLengthNonuniformity, LowGreyLevelRunEmphasis, HighGreyLevelRunEmphasis, ShortRunLowGreyLevelEmphasis, ShortRunHighGreyLevelEmphasis, LongRunLowGreyLevelEmphasis, LongRunHighGreyLevelEmphasis).

#### Data statistics

Each AEF texture group, which comprised all patients, was initially tested using the Kolmogorov-Smirnov Test, to judge whether they fit into a normal distribution. Then, comparisons of AEF texture features were made between groups of “Improved” (CR + PR) and “Un-improved” (SD + PD) patients, as well as between “Un-worsened” (CR + PR + SD) and “Worsened” (PD) patients. An independent sample t test or Mann-Whitney U test was used as appropriate for continuous variables, while a chi-squared test or Fisher’s exact test was used for categorical variables.

To reduce the dimensionality of texture features and avoid the risk of overfitting, the spearman’s rank correlation test was used to exclude the redundant features (correlation coefficient  $|r| \geq 0.9$ ). Afterwards, the Least Absolute Shrinkage and Selection Operator (LASSO) algorithm was performed to identify the most useful features, with penalty parameter tuning conducted by 5-fold cross-validation. A multi-variate logistic regression was performed using the remaining features to estimate an “Improve” or “Un-worsened” outcome. A Receiver Operator Characteristic (ROC) analysis was applied to

assess the discriminative performance of the models, including the area under the curve (AUC), the diagnostic accuracy, the sensitivity, and the specificity. A Calibration Curves Analysis (CCA) and a Decision Curve Analysis (DCA) were also applied, to assess the calibration degree of the models, and to evaluate their net benefit for clinical application at different probability threshold values.

All statistical analyses were performed with R (Version 3.5.1) and Python (Version 3.5.6). A two-tailed  $p < 0.05$  indicated statistical significance.

## Results

### Patient management

Seventy-five patients with liver cancer were initially recruited for this study. Intrahepatic cholangiocarcinoma (ICC,  $n = 3$ ), hepatic metastatic cancer (HMC,  $n = 5$ ), and HCC ( $n = 67$ ) were diagnosed, based on clinical and imaging findings. A small number of HCCs ( $n = 14$ ) were further confirmed by histopathological findings. Fifty-one patients accepted TACE treatment for tumor control, as recommended by the Multiple Disciplinary Team (MDT) seminar. However, four patients were excluded after the operation due to the presence of multiple HCCs ( $n = 1$ ) and visible AVS ( $n = 3$ ) seen on angiography. After discharge, two other patients asked to quit the study for personal reasons. Eventually, forty-five patients completed the imaging follow-up and were ultimately enrolled (CR = 13, PR = 9, SD = 9, PD = 14). Their demographic and clinical characteristics are summarized in (Table 1). A diagram is presented to illustrate the workflow of this study (Fig. 1).

### Image processing

CECT scans took about 5 min on average with no accident occurrence. Neither immediate nor late contrast-related complications arose. C.K. image processing was conducted successfully in all patients. Forty-five HCC lesions were processed, according to the calculation of the largest tumor area by means of multiplying the pixel count and pixel size, the tumor sizes were: (1) Range:  $1.25\text{cm}^2 \sim 73.29\text{cm}^2$ ; (2) Mean  $\pm$  SD:  $10.69 \pm 1.89\text{cm}^2$ ; (3) 95% CI:  $6.70\text{cm}^2 \sim 14.34\text{cm}^2$ . The AEF map showed a good contrast of HCC to normal liver parenchyma, illustrating an elevated proportion of artery/portal perfusion (Fig. 1). Significant differences were found in 8 AEF texture features between “Improved” and “Un-improved” patients (Table 2), while none were observed between “Un-worsened” and “Worsened” patients. Box diagrams of these features were plotted to illustrate their mathematical distribution (Fig. 2).

**Table 1** Baseline of the enrolled cases

Characteristics	Improved	Un-improved	<i>p</i>	Un-worsened	Worsened	<i>p</i>
Gender	18 <sup>Male</sup> /4 <sup>Female</sup>	19 <sup>Male</sup> /4 <sup>Female</sup>	0.945	27 <sup>Male</sup> /4 <sup>Female</sup>	10 <sup>Male</sup> /4 <sup>Female</sup>	0.203
Age (years)	63.00 ± 9.18	60.09 ± 8.98	0.288	61.87 ± 9.14	60.71 ± 9.28	0.698
Weight (kg)	66.91 ± 11.98	70.74 ± 12.81	0.307	70.65 ± 11.87	64.93 ± 13.16	0.155
Hepatitis type	15 <sup>B</sup> /7 <sup>Others</sup>	19 <sup>B</sup> /4 <sup>Others</sup>	0.260	22 <sup>B</sup> /9 <sup>Others</sup>	12 <sup>B</sup> /2 <sup>Others</sup>	0.287
Alcoholic history	11 <sup>Yes</sup> /11 <sup>No</sup>	10 <sup>Yes</sup> /13 <sup>No</sup>	0.661	15 <sup>Yes</sup> /16 <sup>No</sup>	6 <sup>Yes</sup> /8 <sup>No</sup>	0.731
HCC family history	4 <sup>Yes</sup> /18 <sup>No</sup>	6 <sup>Yes</sup> /17 <sup>No</sup>	0.524	4 <sup>Yes</sup> /27 <sup>No</sup>	6 <sup>Yes</sup> /8 <sup>No</sup>	0.025
Tumor stage*	12 <sup>A</sup> /7 <sup>B</sup> /3 <sup>C</sup>	8 <sup>A</sup> /11 <sup>B</sup> /4 <sup>C</sup>	0.596	15 <sup>A</sup> /12 <sup>B</sup> /4 <sup>C</sup>	5 <sup>A</sup> /6 <sup>B</sup> /3 <sup>C</sup>	0.343
Child-Pugh score	5.55 ± 0.67	5.70 ± 0.88	0.523	5.61 ± 0.72	5.64 ± 0.93	0.906
Ammonia (mmol/L)	56.67 ± 18.44	73.35 ± 18.68	0.004	62.86 ± 21.16	70.36 ± 17.49	0.223
Albumin (g/L)	37.42 ± 6.06	35.98 ± 6.12	0.431	37.08 ± 5.63	35.80 ± 7.07	0.517
Total bilirubin (mmol/L)	21.43 ± 8.27	18.71 ± 1.30	0.335	21.38 ± 8.39	17.06 ± 10.93	0.154
Prothrombin time (S)	13.10 ± 1.63	12.63 ± 1.47	0.315	13.09 ± 1.55	12.34 ± 1.47	0.137
AFP (μg/L)	78.04 <sup>(2.10 ~ 11,041.00)</sup>	26.05 <sup>(2.48 ~ 4466.00)</sup>	0.586	78.04 <sup>(2.10 ~ 11,041.00)</sup>	26.03 <sup>(2.48 ~ 4466.00)</sup>	0.364

Note: Description of the baseline clinical data using Mean ± SD for continuous variables that conform to normal distribution, Median<sup>(Range)</sup> for continuous variables that don't conform to normal distribution, and the actual number for categorical variables. Correspondingly, the statistical assessment applied Independent sample t test, Mann-Whitney U test, and Chi-squared test respectively. “\*”: Tumor stages were judged based on Barcelona staging system

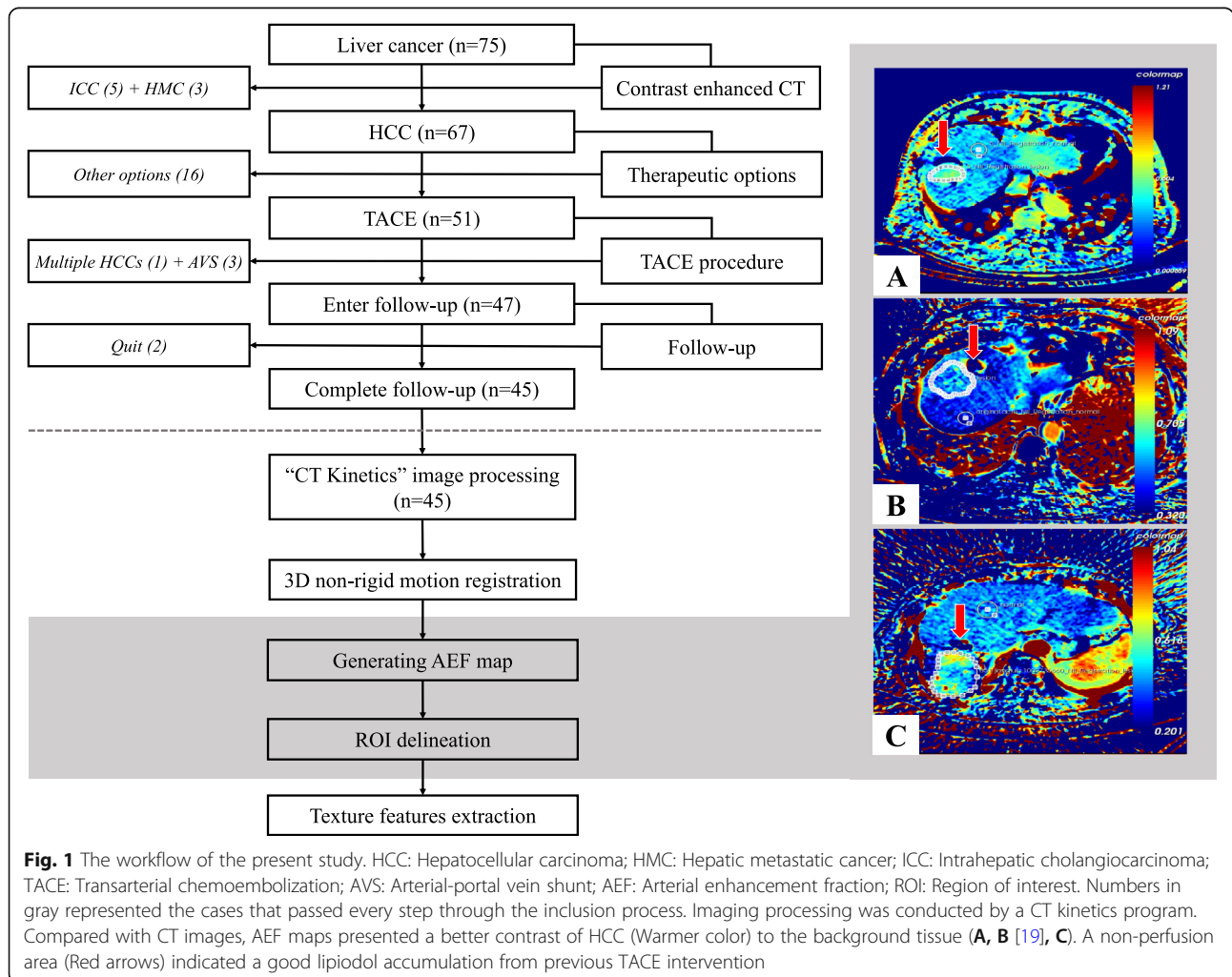


**Fig. 1** The workflow of the present study. HCC: Hepatocellular carcinoma; HMC: Hepatic metastatic cancer; ICC: Intrahepatic cholangiocarcinoma; TACE: Transarterial chemoembolization; AVS: Arterial-portal vein shunt; AEF: Arterial enhancement fraction; ROI: Region of interest. Numbers in gray represented the cases that passed every step through the inclusion process. Imaging processing was conducted by a CT kinetics program. Compared with CT images, AEF maps presented a better contrast of HCC (Warmer color) to the background tissue (A, B [19], C). A non-perfusion area (Red arrows) indicated a good lipiodol accumulation from previous TACE intervention

**Table 2** Comparisons of AEF texture features between “Improved” and “Un-improved” patients

AEF texture features	Improved	Un-improved	U	p
MaxIntensity	17.50 <sup>0.85/0.76</sup>	28.26 <sup>1.54/0.86</sup>	132	0.006
Skewness	18.59 <sup>-0.43/-0.45</sup>	27.22 <sup>1.95/0.33</sup>	156	0.028
Energy	18.14 <sup>0.01/0.01</sup>	27.65 <sup>0.03/0.02</sup>	146	0.015
Entropy	27.00 <sup>6.98/7.12</sup>	19.17 <sup>6.30/6.38</sup>	165	0.046
InverseDifferenceMoment	18.23 <sup>0.46/0.48</sup>	27.57 <sup>0.56/0.55</sup>	148	0.017
HaralickCorrelation	29.05 <sup>1093970.86/965593.50</sup>	17.22 <sup>598050.88/386531.00</sup>	120	0.003
HighGreyLevelRunEmphasis	29.25 <sup>3683.28/3936.19</sup>	16.90 <sup>2072.46/1683.97</sup>	104	0.001
ShortRunHighGreyLevelEmphasis	29.68 <sup>3685.10/3926.28</sup>	16.61 <sup>2033.09/1667.16</sup>	106	0.001

Note: Considering there were 32 texture features overall, only the features with significant between-group distinctions were listed in this table. AEF refers to the Arterial enhancement fraction. Data was described using the format of “Rank Mean<sup>Mean/Median</sup>”. Rank Mean was used to perform the Mann-Whitney U test, Mean and Median were listed as the references to help indicate the distribution of the values

**Data statistics**

As evidenced in the previous section, AEF texture features displayed significant dispersed distribution. Before conducting a logistic regression, all features were standardized to minimize this enormous dispersity. After the redundancy based on correlation analysis, 14 AEF textures were remained for subsequently analysis, including MinIntensity, MaxIntensity, MedianIntensity, Variance, Uniformity, Entropy, Inertia, ClusterShade, ClusterProminence,

HaralickCorrelation, RunLengthNonuniformity, ShortRunLowGreyLevelEmphasis, ShortRunHighGreyLevelEmphasis, and LongRunHighGreyLevelEmphasis. After the LASSO regression analysis, 9 textures in modeling an “Improved” outcome and 4 textures in modeling “Un-worsened” outcome remained with non-zero coefficients (Fig. 3).

Finally, multi-variate logistic regression analyses were conducted using the remaining features. The formulas

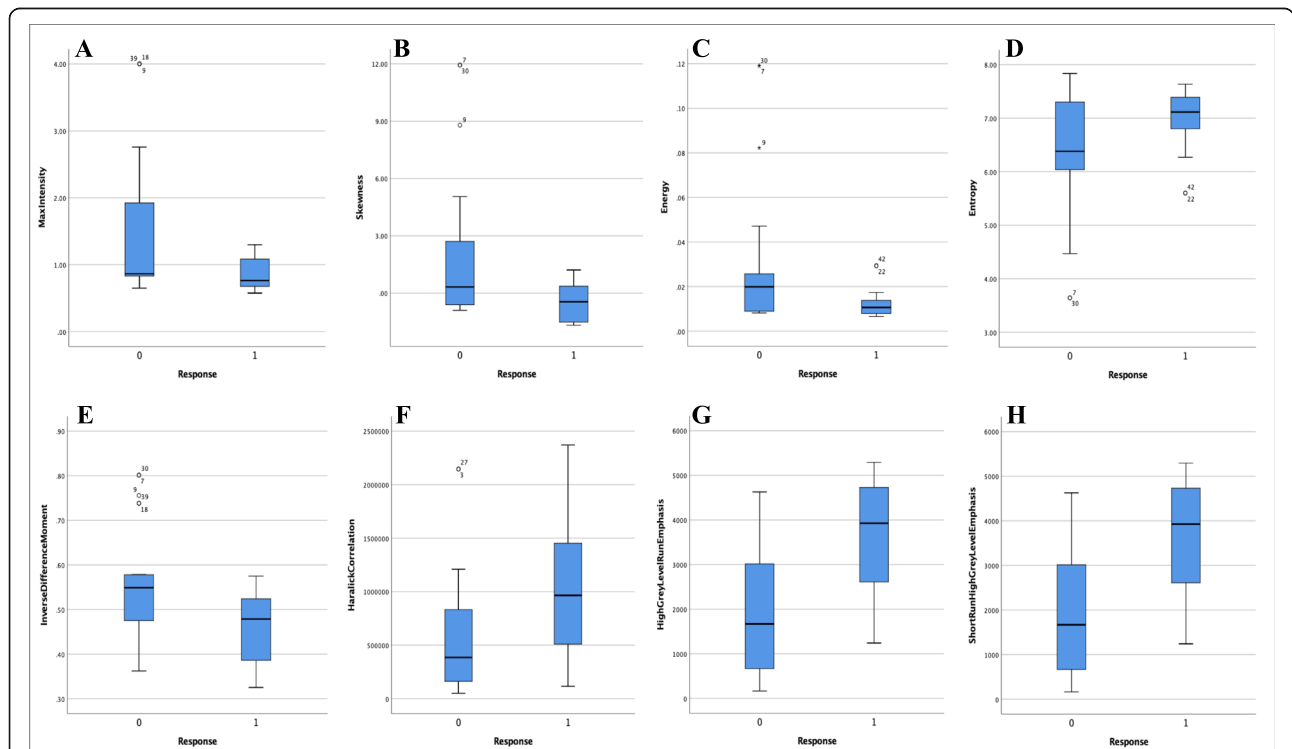


**Fig. 2** Box diagrams showing the difference of AEF texture features ( $p < 0.05$ ) between “Improve” and “Un-improved” patients (Group 0: Un-improved; Group 1: Improved). Based on the definition of each texture, HCCs in “Improved” patients seems to produce more heterogeneous AEF values (C: Lower Energy; D: Higher Entropy; E: Lower InverseDifferenceMoment; H: Higher ShortRunHighGreyLevelEmphasis) and more left-skewed AEF values (B: Lower Skewness; G: Higher HighGreyLevelRunEmphasis), which indicates a more extensive and active angiogenesis, or arterialization, in the tumor

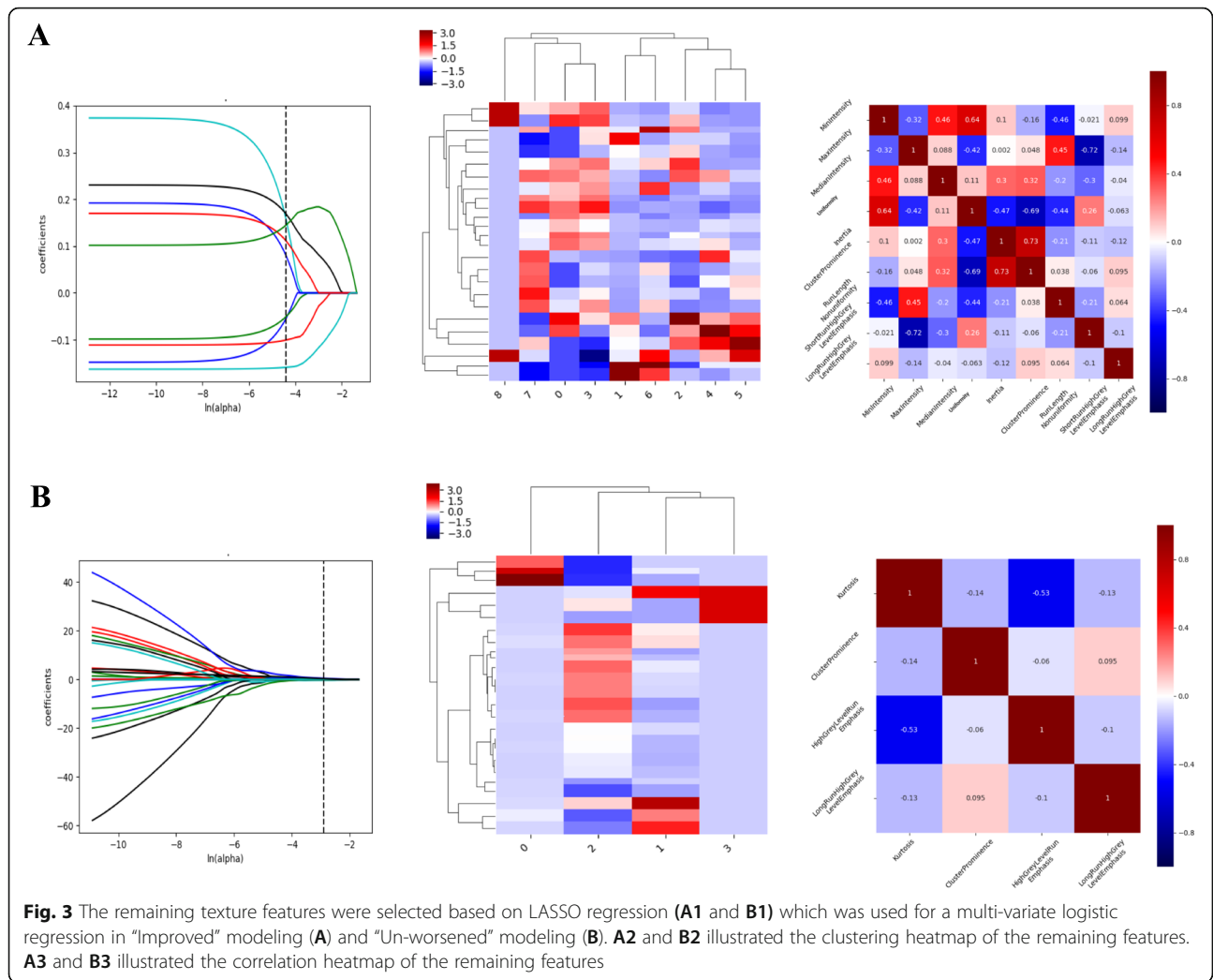
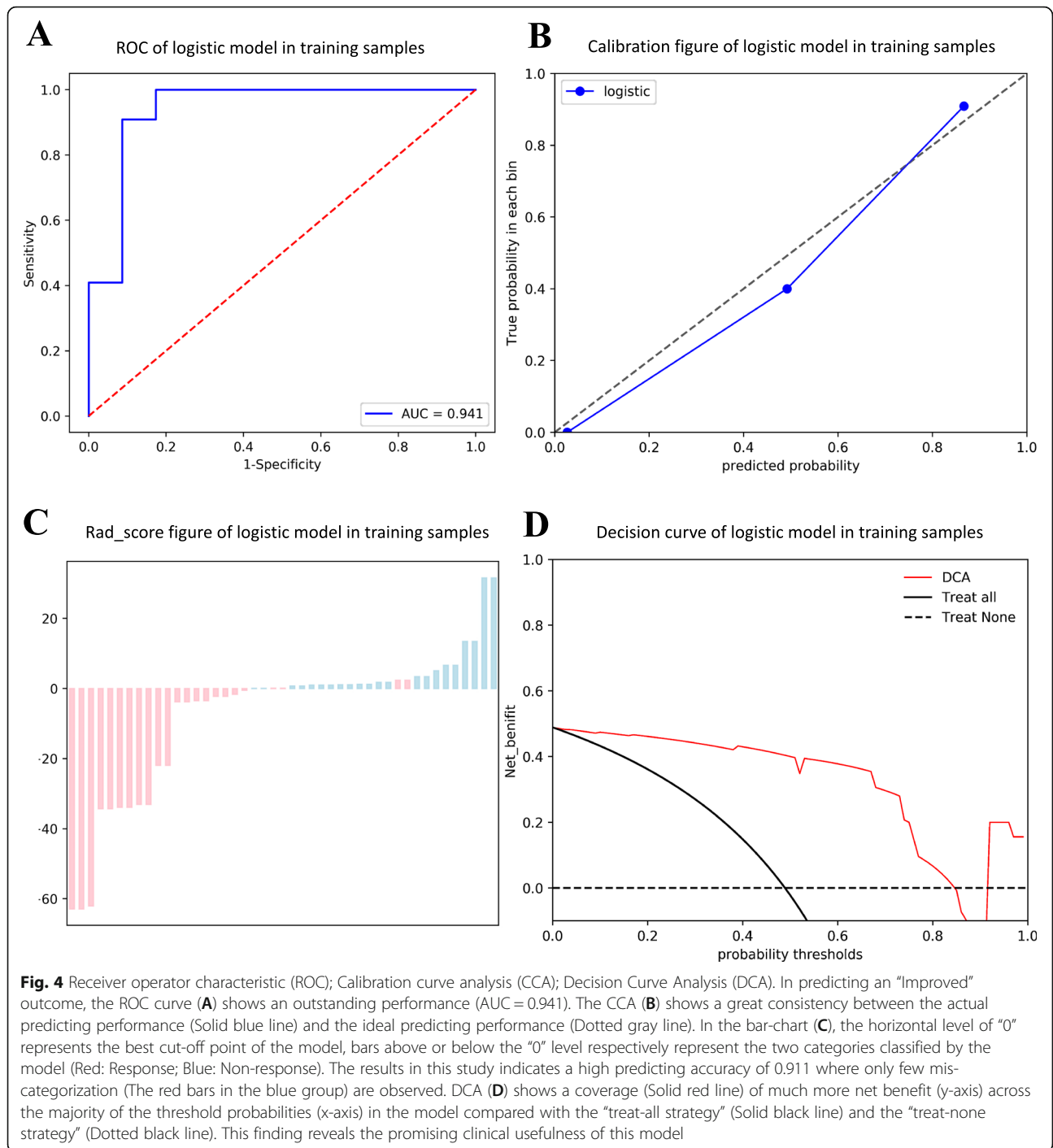


**Table 3** Coefficients of each AEF texture features in two prediction models by multi-variate logistic regression analyses

Model	AUC	Acc.	Sen.	Spe.	Items	Coef.	z	p
A	0.941	0.911	1.000	0.826	Intercept	-7.1555	-0.0000	1.000
					MinIntensity	-8.5860	-1.1469	0.251
					MaxIntensity	-17.1622	-1.1696	0.242
					MedianIntensity	1.9920	0.7683	0.442
					Uniformity	12.5851	1.1778	0.239
					Inertia	4.2988	1.2518	0.211
					ClusterProminence	10.9129	1.2056	0.228
					RunLengthNonuniformity	0.5123	0.3110	0.756
					ShortRunHighGreyLevelEmphasis	-4.6584	-1.0423	0.297
					LongRunHighGreyLevelEmphasis	-12.0604	-0.0000	1.000
B	0.824	0.711	0.581	1.000	Intercept	3.1287	0.0230	0.982
					Kurtosis	-0.5309	-0.8292	0.407
					ClusterProminence	1.8890	1.7340	0.083
					HighGreyLevelRunEmphasis	0.5523	1.1414	0.254
					LongRunHighGreyLevelEmphasis	5.2633	0.0152	0.988

Note: Model A was applied for the prediction of “Improved” outcome; Model B was applied for the prediction of “Un-worsened” outcome. AUC Area Under Curve; Acc. Accuracy; Sen. Sensitivity; Spe. Specificity



for modeling AEF in the prediction of “Improved” (Model A) and “Un-worsened” (Model B) outcomes are shown below with the coefficients listed in (Table 3). The AUC, the diagnostic accuracy, the sensitivity, and the specificity of two models were 0.941, 0.911, 1.000, 0.826 and 0.824, 0.711, 0.581, 1.000, respectively. The prediction performance and the clinical usage of the models are shown in (Fig. 4) and (Fig. 5), respectively.

$$\begin{aligned} \text{Model A : } f_{\text{Improved}} = & -7.1555 - 8.5860 \\ & \times \text{MinIntensity} - 17.1622 \\ & \times \text{MaxIntensity} + 1.9920 \\ & \times \text{MedianIntensity} + 12.5851 \\ & \times \text{Uniformity} + 4.2988 \times \text{Inertia} \\ & + 10.9129 \times \text{ClusterProminence} \\ & + 0.5123 \times \text{RunLengthNonuniformity} \\ & - 4.6584 \\ & \times \text{ShortRunHighGreyLevelEmphasis} \\ & - 12.0606 \\ & \times \text{LongRunHighGreyLevelEmphasis} \end{aligned}$$

$$\begin{aligned} \text{Model B : } f_{\text{Un-worsened}} = & 3.1287 - 0.5309 \times \text{Kutorsis} \\ & + 1.8890 \\ & \times \text{ClusterProminence} \\ & + 0.5523 \\ & \times \text{HighGreyLevelEmphasis} \\ & + 5.2633 \\ & \times \text{LongRunHighGreyLevelEmphasis} \end{aligned}$$

## Discussion

After TACE intervention, an area with dense lipiodol accumulation is regarded as complete necrosis, where no enhancement is meant to be detected. If enhancement is detected, the remaining enhanced area will be judged residual [20, 21]. Although enhanced CT is the most commonly used imaging modality in follow-up [22] appointments, several studies have reported on CT’s limitations of which we should all be aware [23, 24]: (1) Routine enhanced CT can’t provide quantitative data [22]; (2) Lipiodol accumulation can cover or disturb the residual/recurrent enhancement inside/around the tumor [22, 25, 26]; (3) TACE brings the changes in tumor enhancement more often than the changes in tumor size [27]; (4) The devascularization effect of TACE can be heterogeneous and therefore difficult to manually measure [27]. Considering these shortages of routine enhanced CT, AEF can be an optional subject for investigation in the absence of AVS [8, 26, 28] with the following benefits: (1) AEF can improve the detection of HCC and can facilitate the detection of residual/recurrent lesions with faint arterial enhancement or slight wash-out in the portal phase [8, 9]; (2) AEF can successfully overcome the blight of already existing lipiodol because only the area with enhancement can be highlighted and picked out by subtraction [26]; (3) TACE eliminates the feeding artery of HCC so that the

AEF of a tumor decreases while the AEF of liver tissue doesn’t [27]; (4) AEF reflects the status of angiogenesis, which is a vital appearance in tumor histology [29, 30]. These benefits enable us to correlate AEF quantification with survival data [27] and tumor response [31], and also to quantify clinical outcomes by comparing AEF before and after TACE treatment. The findings in other research or clinical trials indeed inspired us in considering the possibility of AEF being able to predict tumor response prior to the actual, invasive operation. This would allow for a comprehensive assessment of the necessity of TACE before it is conducted.

In the present study, we achieved a deeper exploration of AEF by applying texture analysis, which involved multiple detailed mathematical and spatial distribution features far beyond the comprehension of human eyes [32–34]. As introduced in the literature [35, 36], Energy and InverseDifferenceMoment are the textures that measure the homogeneity of an image while Entropy reflects local heterogeneity by specifying the uncertainty or randomness in the image values. Our results showed that those HCCs with a good response to TACE tended to reveal a bigger heterogeneity of AEF, this phenomenon can be explained by the pathophysiological process of HCC development. According to its definition, AEF is qualified to reflect the angiogenesis status of HCC [37–41], where the arterial and portal perfusion changes inversely rather than synchronously. HCC develops from the basic cirrhotic background or normal liver parenchyma where the portal perfusion should be predominant and almost even. The growth and maturation of HCC induces multifocal angiogenesis, more specifically called arterialization. Thus, during HCC development, the portion of arterial perfusion increases in more and more voxels, resulting in not only an elevation of AEF’s average, but also an enlargement of AEF variation among all the HCC voxels. Moreover, skewness measures the asymmetry of the distribution of values towards the Mean value [35, 36], depending on where the tail slants and where the mass of the distribution is concentrated. This mass of distribution can be positive (Right-skewed: Values more concentrated on the left side of the distribution curve, mean > median) or negative (Left-skewed: Values more concentrated on the right side of the distribution curve, mean < median) [42–44]. Among the other features we found distinctions in, HighGreyLevelRunEmphasis, measures the concentration of higher color scales, ShortRunHighGreyLevelEmphasis measures the joint distribution of shorter run lengths in the concentration of higher color scales [35, 36]. Our results indicated a trend of abundant, concentrated, but discontinuous arterialization in more voxels in “Improved” patients. In contrast, “Un-improved” patients revealed a status of continuously poor and scattered



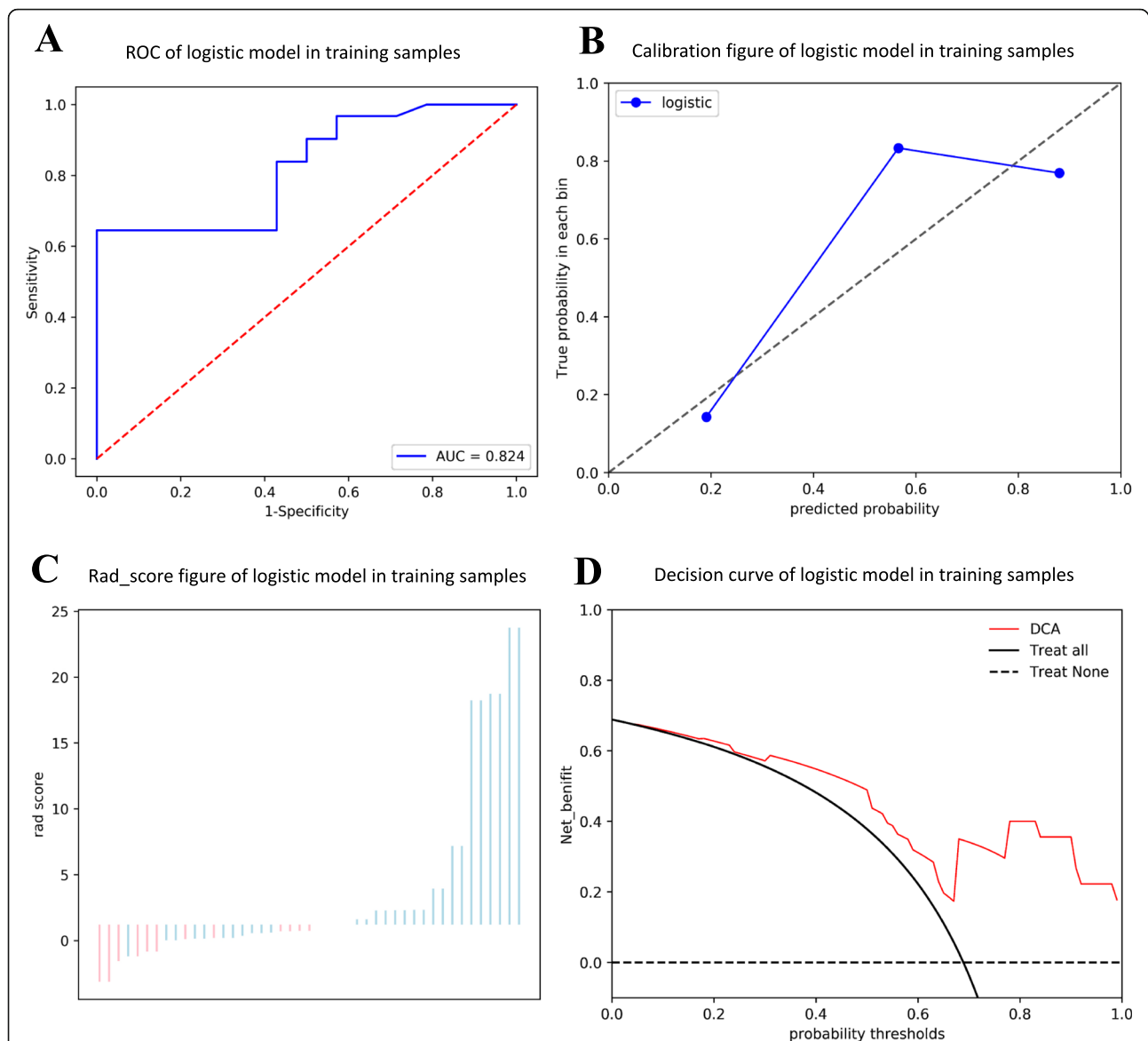


**Fig. 5** Receiver operator characteristic (ROC); Calibration curve analysis (CCA); Decision Curve Analysis (DCA). In predicting a “Un-worsened” outcome, the ROC curve (**A**) shows a good performance (AUC = 0.824). The CCA (**B**) shows a passable consistency between the actual predicting performance (Solid blue line) and the ideal predicting performance (Dotted gray line). The bar-chart (**C**) shows the best cut-off point of this model, which allows for a perfect prediction of a negative outcome (“Worsened”, Blue bar). Yet, the predicting performance for a “Un-worsened” outcome is unsatisfactory because of the presence of multiple false-positive cases, which results in a comprehensive predicting accuracy of 0.711. The DCA (**D**) shows the advantages of this model (Solid red line) compared with the “treat-none strategy” (Dotted black line), while its advantages over the “treat-all strategy” (Dotted black line) are not as significant

arterialization in more voxels. Therefore, we can infer that a lesion of HCC with a more heterogeneous and more left-skewed AEF correlates with a more extensive and active arterialization, which can enhance the tumor staining, facilitate the TACE procedure, and possibly amplify the effect of devascularization. Our personal experience also suggests that sufficient arterialization of HCC can strengthen the confidence in assigning TACE operation to patients and encourage better prognostic expectations.

It is believed that heterogeneity related texture features should be more or less correlated with the histological features of a tumor [45, 46] and, as assumed, be correlated with the biological behavior of a tumor that can influence prognosis. Thus, in order to discover more information about the relationship between AEF texture features and tumor response of HCC to TACE, we implemented a multi-variate logistic regression in which all the AEF textures were initially enrolled. However, consistent with other studies [34, 47, 48], it was necessary to

apply some specific selection strategies to exclude redundant textures, in order to avoid exaggerating the importance of specific textures that had an interacting influence due to overlapping effect. In our research, two AEF based multi-texture models for predicting “Improved” and “Un-worsened” outcomes were successfully built, in which the IBS features, IBH features, GLCM features, and GLRLM features were all covered. These features all describe the mathematical distribution and spatial arrangement of AEF from different perspectives [35, 36]. The IBS and IBH features describe the distribution of pixel intensities within the image region defined by commonly used and basic metrics. The GLCM is a matrix that expresses how combinations of discretized grayscales of neighboring pixels. The GLRLM quantifies grayscale runs, which are defined as the length in number of consecutive pixels that have the same grayscale along a direction. To some extent, our AEF models, covering 4 classes of texture features, could be regarded as ones with comprehensive potential. Impressively, we gained an outstanding performance in encouraging diagnostic accuracy. The sensitivity for predicting “Improved” and the specificity for predicting “Un-worsened” outcome achieved the top value of 100%. In comparison, our results outperformed Zhao’s study [48], where she reported a combined nomogram for predicting early recurrence in HCC after partial hepatectomy in training group, with a diagnostic performance (AUC = 0.878) higher than MRI radiomics model solo (AUC = 0.831) and clinicopathologic radiologic model solo (AUC = 0.797). We attribute the better performance of our AEF models to the application of perfusion processing, which allows non-invasive quantification of hemodynamic information [49, 50] that improves the detection [51, 52], grading [53–55], and monitoring [37, 56] of HCC. Furthermore, perfusion processing can also measure the viable vascular structure of HCC after treatments, which helps in tumor response assessment [57–60] and prediction [61–63], as well as in the prognosis and prediction of survival [64–66]. The novelty of the present study lies in a new methodology where texture analysis is conducted upon perfusion parameters, forming a combination of two sorts of functional imaging applications. Similar methodology was introduced in Liu’s study [47], but it was concerned with brain tumor (Pituitary macroadenoma). Kloth et al. [67] revealed the value of specific enhanced CT textures in predicting tumor response of HCC to DEB-TACE (Drug eluting beads TACE), where the perfusion parameters were applied, however, only to assess the tumor response, which means no perfusion texture features were extracted. Based on our investigation, studies combining perfusion quantification and texture analysis in HCC are still lacking.

Undoubtedly, liver perfusion changes in a certain region when arterial perfusion is exceedingly increased due to highly active arterialization and when portal feeding declines significantly due to the presence of PVTT. However, in our opinion, these factors primarily influence the general perfusion features of liver tissue rather than the AEF texture features of HCC lesions. For example, the hypertrophic feeding artery indeed alters the blood flow velocity and volume (BF and BV) in the tumor. Consequently, the average AEF may also be elevated. However, what AEF texture features describe is the distribution of AEF values in a ROI, which quantifies the mathematical and spatial relationship among these AEF values. These values are neither the mean value nor the sum value. Histologically, the distribution features of AEF only result from differences in arterialization levels between any two adjacent tumor voxels or from differences in the position of a specific arterialization level. Thus, AEF texture features are theoretically decided by histological heterogeneity instead of by total arterial perfusion. On the other hand, HCC is fed basically by arterial neovascularization, especially in the late phase, where there is enough time to allow for significant tumor progression and sufficient arterialization. Therefore, late phase HCCs tend to present such abundant arterial feeding that portal feeding can be too insufficient to be observed. On an AEF map, tumorous tissue can be maximally highlighted due to an abundance of artery feeding. In contrast, although PVTT can block/restrict portal flow, healthy tissue can still be maximally hidden due to a lack of artery feeding. Thus, we do not believe that the presence of PVTT influences the AEF of HCC. Despite this, we do agree that the inherent microcirculation changes of a tumor may correlate with AEF features, which can be revealed by histology. Unfortunately, we did not acquire enough histological data in this study because: [1] According to the current guidelines, HCC can be diagnosed with adequate clinical data including disease history, imaging findings, tumor biomarkers, and so on. Thus, histological data is not necessary for the diagnosis of HCC [2]; Moreover, most participants in this study had been previously treated with multiple therapeutic means like TACE or radiofrequency ablation. These interventions typically produce a certain level of embolus deposition or necrosis inside the tumor, which can render new biopsies unreliable due to a possible false-negative result or inflammation infiltration.

There are several novel findings which are notable in this study: [1] An AEF map converted from CECT images may improve the viable tumor segmentation [2]; Like semi-functional imaging, AEF texture features can better reflect the pathophysiological status of a tumor [3]; The heterogeneity of AEF may imply the tumor response of HCC to TACE [4]; Certain AEF texture

features may be able to influence and predict the tumor response of HCC to TACE [5]; Texture analysis on AEF may help in the selecting optimal HCC patients for TACE intervention. Concurrently, we are also aware of several limitations of this study, apart from the lack of histological data. First, a validation group was not set because of the limited sample size. Second, the lack of standardization in texture analysis is a concerned due to the diversity of imaging equipment, scanning protocols, processing software, and ROI segmentation [68–71]. Finally, we found AEF MaxIntensity and HaralickCorrelation showed between-group distinction, but we were not convinced that they are qualified in demonstrating tumor heterogeneity, because: [1] MaxIntensity represents the single pixel with the highest AEF value in the ROI, which is too independent and individualized to reflect the texture feature of the whole ROI; and, [2] HaralickCorrelation measures the linear dependency of a pixel to its neighboring pixels [72], which can have diverse values between certain adjacent pixels but presents the same overall value for the whole ROI. Therefore, further studies involving more cases and validation group should be encouraged, as more findings on the relationship between the thousands of perfusion texture features and the clinical outcomes of HCC are needed.

## Conclusion

By using perfusion conversion and texture analysis on CECT images, the ability of AEF to influence and predict tumor response in HCC to TACE was demonstrated. AEF can predict tumor response through certain texture features and through its heterogeneity. These findings can improve the selection process of TACE patients and contribute to more favorable outcomes in this intervention.

## Abbreviations

HCC: Hepatocellular carcinoma; TACE: Transarterial chemoembolization; AEF: Arterial enhancement fraction; CECT: Contrast enhanced computed tomography; mRECIST: Modified response evaluation criteria in solid tumours; ROC: Receiver operator characteristic; AUC: Area under curve

## Acknowledgements

Not applicable.

## Authors' contributions

ZM L, XN M, Y G Study design. All authors Data acquisition. XN M, Y G Data analysis. XN M, Y G Data interpretation. XN M, Y G Software application. ZM L Supervision. All authors Writing - original draft. All authors Writing - revise & editing. All authors Submission approval. All authors Accountability.

## Funding

The present study did not receive any funding in the study design, data collection, data analysis, data interpretation, and the writing of the manuscript.

## Availability of data and materials

The data that support the findings of this study are obtained from the Electrical Medical Record (EMR) and Picture Archiving and Communication System (PACS) of Shengjing hospital, which involves a lot of private

information of the participants and particular policies/regulations of Shengjing hospital. Strict restrictions apply to the availability of these data for public sharing. Additionally, the raw data also contain information that other ongoing study is using. Therefore, the raw data can't be publicly shared at this time.

## Declarations

### Ethics approval and consent to participate

Our research, performed in accordance with the principles stated in the Declaration of Helsinki, was approved by the Ethics Committee of Shengjing hospital of China Medical University.

The present study is a retrospective study, where not any interventions beyond routine clinical management were given onto the patients, but only their clinical data were collected and analyzed. We have informed all participants why the research is being conducted, and how the data we are collecting is being stored. Consent was obtained from all patients or their legal clients informing that their clinical data may be used and published in future research with patients' identification anonymized.

### Consent for publication

All authors of the manuscript have read and agreed to its content and are accountable for all aspects of the accuracy and integrity of the manuscript in accordance with ICMJE criteria.

The authors of this study declare that the article is original, has not already been published in a journal, and is not currently under consideration by another journal.

The publication of this submission is approved by all authors, if accepted. It will not be published elsewhere in the same form, in English or in any other language.

### Competing interests

The authors declare that they have no competing interests.

### Author details

<sup>1</sup>Department of Radiology, ShengJing hospital of China Medical University, 12# floor at 1# building, 39 Huaxiang Road, Shenyang City 110000, Liaoning Province, China. <sup>2</sup>GE Healthcare (China), Shanghai, China.

Received: 21 May 2021 Accepted: 19 July 2021

Published online: 12 August 2021

## References

- Bureau of Medical Administration NH, Family Planning Commission of the People's Republic of C. Diagnosis, management, and treatment of hepatocellular carcinoma (V2017). *Zhonghua Gan Zang Bing Za Zhi*. 2017; 25(12):886–95.
- European Association for the Study of the Liver. Electronic address eee, European Association for the Study of the L. EASL clinical practice guidelines: management of hepatocellular carcinoma. *J Hepatol*. 2018;69(1): 182–236. <https://doi.org/10.1016/j.jhep.2018.03.019>.
- Bruix J, Sherman M. Practice guidelines committee AaFtSoLD. Management of hepatocellular carcinoma. *Hepatology*. 2005;42(5):1208–36. <https://doi.org/10.1002/hep.20933>.
- Di Maio M, Daniele B, Gallo C, Perrone F. Re: design and endpoints of clinical trials in hepatocellular carcinoma. *J Natl Cancer Inst*. 2008;100(21): 1557; author reply 1557–1558–1557; author reply 1558. <https://doi.org/10.1093/jnci/djn341>.
- Park YN, Yang CP, Fernandez GJ, Cubukcu O, Thung SN, Theise ND. Neoangiogenesis and sinusoidal "capillarization" in dysplastic nodules of the liver. *Am J Surg Pathol*. 1998;22(6):656–62. <https://doi.org/10.1097/0000478-199806000-00002>.
- Hayashi M, Matsui O, Ueda K, Kawamori Y, Kadoya M, Yoshikawa J, et al. Correlation between the blood supply and grade of malignancy of hepatocellular nodules associated with liver cirrhosis: evaluation by CT during intraarterial injection of contrast medium. *AJR Am J Roentgenol*. 1999;172(4):969–76. <https://doi.org/10.2214/ajr.172.4.10587130>.
- Tajima T, Honda H, Taguchi K, Asayama Y, Kuroiwa T, Yoshimitsu K, et al. Sequential hemodynamic change in hepatocellular carcinoma and dysplastic nodules: CT angiography and pathologic correlation. *AJR Am J Roentgenol*. 2002;178(4):885–97. <https://doi.org/10.2214/ajr.178.4.1780885>.

8. Kim KW, Lee JM, Klotz E, Park HS, Lee DH, Kim JY, et al. Quantitative CT color mapping of the arterial enhancement fraction of the liver to detect hepatocellular carcinoma. *Radiology*. 2009;250(2):425–34. <https://doi.org/10.1148/radiol.2501072196>.
9. Huber AT, Schuster F, Ebner L, Bütikofer Y, Ott D, Leidolt L, et al. Hepatocellular carcinoma screening with computed tomography using the arterial enhancement fraction with radiologic-pathologic correlation. *Investig Radiol*. 2016;51(1):25–32. <https://doi.org/10.1097/RLI.0000000000000201>.
10. Gillies RJ, Kinahan PE, Hricak H. Radiomics: images are more than pictures, they are data. *Radiology*. 2016;278(2):563–77. <https://doi.org/10.1148/radiol.2015151169>.
11. Kumar V, Gu Y, Basu S, Berglund A, Eschrich SA, Schabath MB, et al. Radiomics: the process and the challenges. *Magn Reson Imaging*. 2012; 30(9):1234–48. <https://doi.org/10.1016/j.mri.2012.06.010>.
12. Scalco E, Rizzo G. Texture analysis of medical images for radiotherapy applications. *Br J Radiol*. 2017;90(1070):20160642. <https://doi.org/10.1259/bjr.20160642>. Epub 2016 Nov 25.
13. Brooks FJ. On some misconceptions about tumor heterogeneity quantification. *Eur J Nucl Med Mol I*. 2013;40(8):1292–4. <https://doi.org/10.1007/s00259-013-2430-y>.
14. Liu SL, Liu S, Ji CF, Zheng H, Pan X, Zhang Y, et al. Application of CT texture analysis in predicting histopathological characteristics of gastric cancers. *Eur Radiol*. 2017;27(12):4951–9. <https://doi.org/10.1007/s00330-017-4881-1>.
15. Child CG, Turcotte JG. Surgery and portal hypertension. *Major Probl Clin Surg*. 1964;1:1–85.
16. Pugh RN, Murray-Lyon IM, Dawson JL, Pietroni MC, Williams R. Transection of the oesophagus for bleeding oesophageal varices. *Br J Surg*. 1973;60(8): 646–9. <https://doi.org/10.1002/bjs.1800600817>.
17. Chen ZP, Shi ZZ, Li YG, Guo Y, Tong D. Post-processing of computed tomography perfusion in patients with acute cerebral ischemia: variability of inter-reader, inter-region of interest, inter-input model, and inter-software. *Eur Radiol*. 2020;30(12):6561–9. <https://doi.org/10.1007/s00330-020-07000-7>.
18. Lee DH, Lee JM, Klotz E, Han JK. Multiphasic dynamic computed tomography evaluation of liver tissue perfusion characteristics using the dual maximum slope model in patients with cirrhosis and hepatocellular carcinoma: a feasibility study. *Investig Radiol*. 2016;51(7):430–4. <https://doi.org/10.1097/RLI.0000000000000247>.
19. Mao XN, Guo Y, Lu ZM, Wen F, Liang HY, Sun W. Enhanced CT textures derived from computer mathematic distribution analysis enables arterial enhancement fraction being an imaging biomarker option of hepatocellular carcinoma. *Front Oncol*. 2020;10:1337. <https://doi.org/10.3389/fonc.2020.01337>. eCollection 2020.
20. Takayasu K, Arii S, Matsuo N, Yoshikawa M, Ryu M, Takasaki K, et al. Comparison of CT findings with resected specimens after chemoembolization with iodized oil for hepatocellular carcinoma. *AJR Am J Roentgenol*. 2000;175(3):699–704. <https://doi.org/10.2214/ajr.175.3.1750699>.
21. Mannelli L, Kim S, Hajdu CH, Babb JS, Clark TW, Taouli B. Assessment of tumor necrosis of hepatocellular carcinoma after chemoembolization: diffusion-weighted and contrast-enhanced MRI with histopathologic correlation of the explanted liver. *AJR Am J Roentgenol*. 2009;193(4):1044–52. <https://doi.org/10.2214/AJR.08.1461>.
22. Tsui EY, Chan JH, Cheung YK, et al. Evaluation of therapeutic effectiveness of transarterial chemoembolization for hepatocellular carcinoma: correlation of dynamic susceptibility contrast-enhanced echoplanar imaging and hepatic angiography. *Clin Imaging*. 2000;24(4):210–6. [https://doi.org/10.1016/S0899-7071\(00\)00204-7](https://doi.org/10.1016/S0899-7071(00)00204-7).
23. Jang KM, Choi D, Lim HK, Lim JH, Lee JY, Lee WJ, et al. Depiction of viable tumor in hepatocellular carcinoma treated with transarterial chemoembolization: multiphasic helical CT with review of the previous serial CT images. *Korean J Radiol*. 2005;6(3):153–60. <https://doi.org/10.3348/kjr.2005.6.3.153>.
24. Kim YS, Rhim H, Lim HK, Park CK, Lee WJ, Do YS, et al. Completeness of treatment in hepatocellular carcinomas treated with image-guided tumor therapies: evaluation of positive predictive value of contrast-enhanced CT with histopathologic correlation in the explanted liver specimen. *J Comput Assist Tomogr*. 2006;30(4):578–82. <https://doi.org/10.1097/00004728-200607000-00005>.
25. Willatt JM, Hussain HK, Adusumilli S, Marrero JA. MR imaging of hepatocellular carcinoma in the cirrhotic liver: challenges and controversies. *Radiology*. 2008;247(2):311–30. <https://doi.org/10.1148/radiol.2472061331>.
26. Lee DH, Lee JM, Klotz E, Kim SJ, Kim KW, Han JK, et al. Detection of recurrent hepatocellular carcinoma in cirrhotic liver after transcatheter arterial chemoembolization: value of quantitative color mapping of the arterial enhancement fraction of the liver. *Korean J Radiol*. 2013;14(1):51–60. <https://doi.org/10.3348/kjr.2013.14.1.51>.
27. Bonekamp S, Bonekamp D, Geschwind JF, et al. Response stratification and survival analysis of hepatocellular carcinoma patients treated with intra-arterial therapy using MR imaging-based arterial enhancement fraction. *J Magn Reson Imaging*. 2014;40(5):1103–11. <https://doi.org/10.1002/jmri.24465>.
28. Kim HC, Kim AY, Han JK, Chung JW, Lee JY, Park JH, et al. Hepatic arterial and portal venous phase helical CT in patients treated with transcatheter arterial chemoembolization for hepatocellular carcinoma: added value of unenhanced images. *Radiology*. 2002;225(3):773–80. <https://doi.org/10.1148/radiol.2253011346>.
29. Gholizadeh N, Simpson J, Ramadan S, Lau P, Greer P. Assessment of prostate tumor heterogeneity using machine learning: an emerging imaging tool for clinical practice. *Asia-Pac J Clin Oncol*. 2018;14:13.
30. Lubner MG, Stabo N, Abel EJ, del Rio AM, Pickhardt PJ. CT textural analysis of large primary renal cell carcinomas: pretreatment tumor heterogeneity correlates with histologic findings and clinical outcomes. *Am J Roentgenol*. 2016;207(1):96–105. <https://doi.org/10.2214/AJR.15.15451>.
31. Chen G, Ma DQ, He W, Zhang BF, Zhao LQ. Computed tomography perfusion in evaluating the therapeutic effect of transarterial chemoembolization for hepatocellular carcinoma. *World J Gastroenterol*. 2008;14(37):5738–43. <https://doi.org/10.3748/wjg.14.5738>.
32. Davnall F, Yip CS, Ljungqvist G, et al. Assessment of tumor heterogeneity: an emerging imaging tool for clinical practice? *Insights Imaging*. 2012;3(6): 573–89. <https://doi.org/10.1007/s13244-012-0196-6>.
33. Ng F, Ganeshan B, Kozarski R, Miles KA, Goh V. Assessment of primary colorectal cancer heterogeneity by using whole-tumor texture analysis: contrast-enhanced CT texture as a biomarker of 5-year survival. *Radiology*. 2013;266(1):177–84. <https://doi.org/10.1148/radiol.12120254>.
34. Han L, Wang S, Miao Y, Shen H, Guo Y, Xie L, et al. MRI texture analysis based on 3D tumor measurement reflects the IDH1 mutations in gliomas - a preliminary study. *Eur J Radiol*. 2019;112:169–79. <https://doi.org/10.1016/j.ejrad.2019.01.025>.
35. van Griethuysen JJM, Fedorov A, Parmar C, Hosny A, Aucoin N, Narayan V, et al. Computational Radiomics system to decode the radiographic phenotype. *Cancer Res*. 2017;77(21):E104–7. <https://doi.org/10.1158/0008-5472.CAN-17-0339>.
36. Zwanenburg A, Vallières M, Abdalah MA, et al. The image biomarker standardization initiative: standardized quantitative Radiomics for high-throughput image-based phenotyping. *Radiology*. 2020;295(2):328–38. <https://doi.org/10.1148/radiol.2020191145>.
37. Mahnken AH, Klotz E, Schreiber S, Bruners P, Isfort P, Günther RW, et al. Volumetric arterial enhancement fraction predicts tumor recurrence after hepatic radiofrequency ablation of liver metastases: initial results. *Am J Roentgenol*. 2011;196(5):W573–9. <https://doi.org/10.2214/AJR.10.4410>.
38. Ippolito D, Sironi S, Pozzi M, Antolini L, Invernizzi F, Ratti L, et al. Perfusion CT in cirrhotic patients with early stage hepatocellular carcinoma: assessment of tumor-related vascularization. *Eur J Radiol*. 2010;73(1):148–52. <https://doi.org/10.1016/j.ejrad.2008.10.014>.
39. Ippolito D, Sironi S, Pozzi M, Antolini L, Ratti L, Alberzoni C, et al. Hepatocellular carcinoma in cirrhotic liver disease: functional computed tomography with perfusion imaging in the assessment of tumor vascularization. *Acad Radiol*. 2008;15(7):919–27. <https://doi.org/10.1016/j.acra.2008.02.005>.
40. Folkman J. Is angiogenesis an organizing principle in biology and medicine? *J Pediatr Surg*. 2007;42(1):1–11. <https://doi.org/10.1016/j.jpedsurg.2006.09.048>.
41. Shan YF, Huang YL, Xie YK, Tan YH, Chen BC, Zhou MT, et al. Angiogenesis and clinicopathologic characteristics in different hepatocellular carcinoma subtypes defined by EpCAM and alpha-fetoprotein expression status. *Med Oncol*. 2011;28(4):1012–6. <https://doi.org/10.1007/s12032-010-9600-6>.
42. Hopkins KD, Weeks DL. Tests for normality and measures of skewness and kurtosis - their place in research reporting. *Educ Psychol Meas*. 1990;50(4): 717–29. <https://doi.org/10.1177/0013164490504001>.
43. Macgillivray HL. Skewness and asymmetry - measures and orderings. *Ann Stat*. 1986;14(3):994–1011.
44. Groeneveld RA, Meeden G. Measuring skewness and kurtosis. *Statistician*. 1984;33(4):391–9. <https://doi.org/10.2307/2987742>.

45. Bashir U, Siddique MM, Mclean E, Goh V, Cook GJ. Imaging heterogeneity in lung Cancer: techniques, applications, and challenges. *Am J Roentgenol*. 2016;207(3):534–43. <https://doi.org/10.2214/AJR.15.15864>.
46. Ganeshan B, Miles KA. Quantifying tumour heterogeneity with CT. *Cancer Imaging*. 2013;13(1):140–9. <https://doi.org/10.1102/1470-7330.2013.0015>.
47. Liu YYQ, Gao BB, Dong B, Padikkalandy Cheriya SS, Song QW, Xu B, et al. Preoperative vascular heterogeneity and aggressiveness assessment of pituitary macroadenoma based on dynamic contrast-enhanced MRI texture analysis. *Eur J Radiol*. 2020;129:109125. <https://doi.org/10.1016/j.ejrad.2020.109125>.
48. Zhao Y, Wu JJ, Zhang QH, et al. Radiomics analysis based on multiparametric MRI for predicting early recurrence in hepatocellular carcinoma after partial hepatectomy. *J Magn Reson Imaging*. 2021;53(4):1066–79. <https://doi.org/10.1002/jmri.27424>. Epub 2020 Nov 20.
49. Cuenod CA, Leconte I, Siauve N, Resten A, Dromain C, Poulet B, et al. Early changes in liver perfusion caused by occult metastases in rats: detection with quantitative CT. *Radiology*. 2001;218(2):556–61. <https://doi.org/10.1148/radiology.218.2.r01fe10556>.
50. Ippolito D, Bonaffini PA, Capraro C, Leni D, Corso R, Sironi S. Viable residual tumor tissue after radiofrequency ablation treatment in hepatocellular carcinoma: evaluation with CT perfusion. *Abdom Imaging*. 2013;38(3):502–10. <https://doi.org/10.1007/s00261-012-9924-0>.
51. Fischer MA, Kartalis N, Grigoriadis A, Loizou L, Stål P, Leidner B, et al. Perfusion computed tomography for detection of hepatocellular carcinoma in patients with liver cirrhosis. *Eur Radiol*. 2015;25(11):3123–32. <https://doi.org/10.1007/s00330-015-3732-1>.
52. Taouli B, Johnson RS, Hajdu CH, Oei MTH, Merad M, Yee H, et al. Hepatocellular carcinoma: perfusion quantification with dynamic contrast-enhanced MRI. *Am J Roentgenol*. 2013;201(4):795–800. <https://doi.org/10.2214/AJR.12.9798>.
53. Chen J, Chen CY, Xia CC, Huang Z, Zuo P, Stemmer A, et al. Quantitative free-breathing dynamic contrast-enhanced MRI in hepatocellular carcinoma using gadoxetic acid: correlations with Ki67 proliferation status, histological grades, and microvascular density. *Abdom Radiol*. 2018;43(6):1393–403. <https://doi.org/10.1007/s00261-017-1320-3>.
54. Jajamovich GH, Huang W, Besa C, Li X, Afzal A, Dyvorne HA, et al. DCE-MRI of hepatocellular carcinoma: perfusion quantification with Tofts model versus shutter-speed model-initial experience. *Magn Reson Mater Phys*. 2016;29(1):49–58. <https://doi.org/10.1007/s10334-015-0513-4>.
55. Sahani DV, Holalkere NS, Mueller PR, Zhu AX. Advanced hepatocellular carcinoma: CT perfusion of liver and tumor tissue - initial experience. *Radiology*. 2007;243(3):736–43. <https://doi.org/10.1148/radiol.2433052020>.
56. Wimmer T, Steiner J, Talakic E, Stauber R, Quehenberger F, Portugaller RH, et al. Computed tomography perfusion following Transarterial chemoembolization of hepatocellular carcinoma: a feasibility study in the early period. *J Comput Assist Tomo*. 2017;41(5):708–12. <https://doi.org/10.1097/RCT.0000000000000592>.
57. Ippolito D, Bonaffini PA, Ratti L, Antolini L, Corso R, Fazio F, et al. Hepatocellular carcinoma treated with transarterial chemoembolization: dynamic perfusion-CT in the assessment of residual tumor. *World J Gastroenterol*. 2010;16(47):5993–6000. <https://doi.org/10.3748/wjg.v16.i47.5993>.
58. Marquez HP, Karalli A, Haubenreisser H, Mathew RP, Alkadhi H, Brismar TB, et al. Computed tomography perfusion imaging for monitoring transarterial chemoembolization of hepatocellular carcinoma. *Eur J Radiol*. 2017;91:160–7. <https://doi.org/10.1016/j.ejrad.2017.03.014>.
59. Tamandl D, Waneck F, Sieghart W, Unterhumer S, Kölblinger C, Baltzer P, et al. Early response evaluation using CT-perfusion one day after transarterial chemoembolization for HCC predicts treatment response and long-term disease control. *Eur J Radiol*. 2017;90:73–80. <https://doi.org/10.1016/j.ejrad.2017.02.032>.
60. Borgheresi A, Gonzalez-Aguirre A, Brown KT, Getrajdman GI, Erinjeri JP, Covey A, et al. Does enhancement or perfusion on Preprocedure CT predict outcomes after embolization of hepatocellular carcinoma? *Acad Radiol*. 2018;25(12):1588–94. <https://doi.org/10.1016/j.acra.2018.02.027>.
61. Ippolito D, Trattenero C, Franzesi CT, et al. Dynamic contrast-enhanced magnetic resonance imaging with gadolinium Ethoxybenzyl Diethylenetriamine Pentaacetic acid for quantitative assessment of vascular effects on hepatocellular-carcinoma lesions treated by Transarterial chemoembolization or radiofrequency ablation. *J Comput Assist Tomo*. 2016;40(5):692–700.
62. Liang PC, Ch'ang HJ, Hsu C, Chen LT, Shih TTF, Liu TW. Perfusion parameters of dynamic contrast-enhanced magnetic resonance imaging predict outcomes of hepatocellular carcinoma receiving radiotherapy with or without thalidomide. *Hepatol Int*. 2015;9(2):258–68. <https://doi.org/10.1007/s12072-014-9557-1>.
63. Yuan Z, Li WT, Ye XD, Zhu HY, Peng WJ. Novel functional magnetic resonance imaging biomarkers for assessing response to therapy in hepatocellular carcinoma. *Clin Transl Oncol*. 2014;16(7):599–605. <https://doi.org/10.1007/s12094-013-1147-5>.
64. Lee SH, Hayano K, Zhu AX, Sahani DV, Yoshida H. Water-exchange-modified kinetic parameters from dynamic contrast-enhanced MRI as prognostic biomarkers of survival in advanced hepatocellular carcinoma treated with antiangiogenic monotherapy. *PLoS One*. 2015;10(9):e0136725. <https://doi.org/10.1371/journal.pone.0136725>. eCollection 2015.
65. Lee SH, Hayano K, Zhu AX, Sahani DV, Yoshida H. Dynamic contrast-enhanced MRI kinetic parameters as prognostic biomarkers for prediction of survival of patient with advanced hepatocellular carcinoma: a pilot comparative study. *Acad Radiol*. 2015;22(11):1344–60. <https://doi.org/10.1016/j.acra.2015.05.012>.
66. Chen BB, Hsu CY, Yu CW, Liang PC, Hsu C, Hsu CH, et al. Dynamic contrast-enhanced MR imaging of advanced hepatocellular carcinoma: comparison with the liver parenchyma and correlation with the survival of patients receiving systemic therapy. *Radiology*. 2016;281(2):454–64. <https://doi.org/10.1148/radiol.2016152659>.
67. Kloth C, Thaiss WM, Kargel R, et al. Evaluation of texture analysis parameter for response prediction in patients with hepatocellular carcinoma undergoing drug-eluting bead Transarterial chemoembolization (DEB-TACE) using biphasic contrast-enhanced CT image data: correlation with liver perfusion CT. *Acad Radiol*. 2017;24(11):1352–63. <https://doi.org/10.1016/j.acra.2017.05.006>.
68. Kim YK, Lee WJ, Park MJ, Kim SH, Rhim H, Choi D. Hypovascular Hypointense nodules on hepatobiliary phase Gadoxetic acid-enhanced MR images in patients with cirrhosis: potential of DW imaging in predicting progression to Hypervascular HCC. *Radiology*. 2012;265(1):104–14. <https://doi.org/10.1148/radiol.12112649>.
69. Kitao A, Matsui O, Yoneda N, Kozaka K, Kobayashi S, Koda W, et al. Hypervascular hepatocellular carcinoma: correlation between biologic features and signal intensity on Gadoxetic acid-enhanced MR images. *Radiology*. 2012;265(3):780–9. <https://doi.org/10.1148/radiol.12120226>.
70. Choi JW, Lee JM, Kim SJ, Yoon JH, Baek JH, Han JK, et al. Hepatocellular carcinoma: imaging patterns on Gadoxetic acid-enhanced MR images and their value as an imaging biomarker. *Radiology*. 2013;267(3):776–86. <https://doi.org/10.1148/radiol.13120775>.
71. Rosenkrantz AB, Pinnamaneni N, Kierans AS, Ream JM. Hypovascular hepatic nodules at gadoxetic acid-enhanced MRI: whole-lesion hepatobiliary phase histogram metrics for prediction of progression to arterial-enhancing hepatocellular carcinoma. *Abdom Radiol*. 2016;41(1):63–70. <https://doi.org/10.1007/s00261-015-0610-x>.
72. Haralick RM, Shanmugam K, Dinstein I. Textural features for image classification. *IEEE T Syst Man Cyb*. 1973;3(6):610–21.

## Publisher's Note

Springer Nature remains neutral with regard to jurisdictional claims in published maps and institutional affiliations.

**Ready to submit your research? Choose BMC and benefit from:**

- fast, convenient online submission
- thorough peer review by experienced researchers in your field
- rapid publication on acceptance
- support for research data, including large and complex data types
- gold Open Access which fosters wider collaboration and increased citations
- maximum visibility for your research: over 100M website views per year

**At BMC, research is always in progress.**

Learn more [biomedcentral.com/submissions](https://biomedcentral.com/submissions)

